Supplementary Material

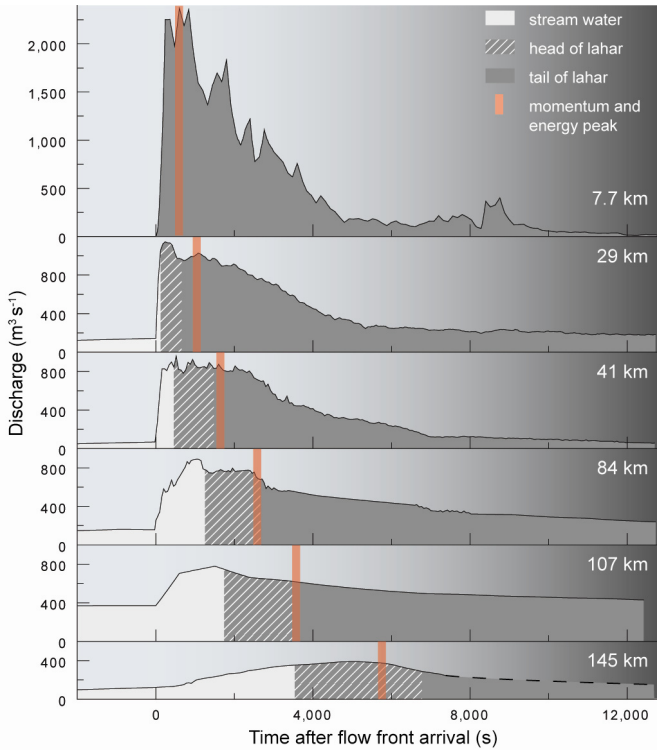

Supplementary Figure DR1. Spatial evolution of the Ruapehu 2007 lahar wave, with discharge shown as a function of arrival time at six stations between 7.7 and 145 km from the Crater Lake dam source. The lahar wave remained a kinematic form until 107 km before dissipating over the remaining c. 90 km travel to the Tasman Sea.
The orange bar depicts the joined peak of linear momentum and energy (both per unit length of lahar). Note the progressive divergence of initially coinciding peaks in discharge and momentum with travel distance to at least 107 km from the Crater Lake dam source.

Instrument; Method	Measured Parameter	Sampling Frequency / Resolution	Deployment	Deduced parameter
Acoustic Flow Monitors (single-band geophones with AFM board; e.g. Hadley and LaHusen, 1995)	• Real-time seismic amplitude in two separate (high and low gain) channels	5 seconds / <1-100 Hz	• on river bank	• lahar arrival time T_A (*) and lahar front velocity U_A (*) through differentiating best-fit power laws of all T_A vs. distance data • peak sediment concentration time T_S (Cole 2011) (*)
Guralp CMG-6TD 3-component broadband seismometers	• ground vibrations up to Nyquist frequency (62.5 Hz) • seismic amplitude • frequency response •signal directionality	Down-sampled to10 seconds / 0.033-60 Hz	• on river bank, N-axis aligned parallel to riverbank	• lahar arrival time T_A (*) and lahar front velocity U_A (*) through differentiating best-fit powerlaws of all T_A vs. distance data • peak sediment concentration time T_S (e.g. Cole 2011) (*)
Digital Video Cameras; Particle-Image-Velocimetry on paired images	• Mid-channel surface velocity U_S (e.g. Doyle et al. 2011)	Paired images at 25 fps every 30 seconds / 0.05 m/s	• pole- or tripod- mounted at bridges and riverbanks	• body velocity U_D (*) assuming a logarithmic velocity profile and the relationship $U_S=kU_D$, where k=0.75 (e.g. Doyle et al. 2011) • local Manning's n (*) through Manning's formula ($n=S^{0.5}R^{2/3}/U_D$) and independent measurements of U_S, pre-lahar channel slope S, and the hydraulic radius R at peak stage. • discharge $Q_I=U_DA$ (*)
Gas bubbler	• Crater Lake Level	6 seconds	• in Crater Lake	• Initial dam-break hydrograph (*) through numerical modeling of flow through a broad-crested weir and constraining breach growth through automated still camera (Manville 2001)
Ultrasonic and Laser Stage Gauges	• Flow height	30 and 60 seconds, except for 107 and 145 km stations were sampling rate was 300 and 120 seconds, respectively, and intermediate stage values were determined from video	• mounted to bridges at mid-channel positions with datum calibrated to stable (preferably hard rock) pre-lahar cross-sections; larger depositional cross-section changes (<<5% of channel capacity) occurred after the interval (T_A, T_M) considered here.	• Wetted perimeter p and wetted area A (*) • hydraulic radii h and R (*) • lahar arrival time T_A (*) and lahar front velocity U_A (*) through differentiating best-fit power laws of all T_A vs. distance data • lahar peak flow time T_Q (*) and lahar peak flow velocity U_Q (*)
Pore-pressure Cell	• Flow depth	5 seconds	• mounted into cylindrical holes drilled into solid river bed	• Wetted perimeter p and wetted area A • hydraulic radii h and R • lahar arrival time T_A (*) • lahar peak flow time T_Q (*) and lahar peak flow velocity U_Q (*)
• Time-series dip sampling, incl. • Water chemistry through: Ion Chromatography, Atomic Absorption Spectroscopy • Sediment characteristics through: Standard Sieving, Laser Particle Sizing, Particle componentry and density analysis	• Sediment weight and volume percentages • Sediment concentration peak time T_S • Sediment grain-size distribution • Water Chemistry (Mg, F, Cl, SO4, Br, pH) • Water conductivity	10 – 600 seconds (depending on flow variation) before lahar arrival, during first 2-4.5 hours after lahar arrival; daily samples for lahar tail during next 5 days	• 2-4 kg time-series dip samples of suspended sediment-water mixtures from upper 1 m of active flow at channel thalweg (e.g. Pierson and Scott, 1985; Scott, 1988; Rodolfo et al., 1996; Dinehart, 1997; Cronin et al., 1997; Lavigne and Suwa, 2004) • samples were filled into plastic bottles, sealed and analyzed in the laboratory	• volumetric Crater-Lake water/stream water ratio (*); (Lube et al. 2009; Christenson et al. 2010); Supplementary material "Calculations of bulk energy and bulk linear momentum" • time-variant mass flux of Crater-Lake water Q_{CLW} (*) (Supplementary material "Calculations of bulk energy and bulk linear momentum")
Airborne LiDAR	Semi-Continuous digitial elevation data	Pre and post lahar / 0.1 m horizontal	• covering first 62 km of Whangaehu River channel	• spatial net-volume geomorphic change (Procter et al. 2010)
Real-Time Kinetic GPS	• Channel cross-sections • Channel slope S • Post-lahar super elevations • Post-lahar peak flow tide lines	Pre and post lahar / 3 cm horizontal	• at regular intervals for entire Whangaehu River channel	• alternative estimate of peak flow velocity (Chow, 1959; Pierson and Scott 1985) • stage/wetted perimeter, stage/wetted area and stage/hydraulic radii relationships (*)
Tripwire	Lahar arrival time	1 measurement	• at a single location in upper Whangaehu channel 1.9 km from Crater Lake	• lahar arrival time T_A (*) and lahar front velocity U_A (*) through differentiating best-fit power laws of all T_A vs. distance data

Supplementary material Table DR1: List of instruments deployed, parameters measured, sample frequency, instrument deployment specifications and deduced parameters to obtain hydrological, sedimentological, kinematic and chemical time-series data for the 18 March 2007 lahar. (*) denotes parameters that were used in this study.

Supplementary Material: Calculations of bulk energy and bulk linear momentum

In Figure 4A we show computed data of bulk flow energy, E_{TOT}, of the frontal part of lahar that contains original Crater Lake water of mass M_0 from several lahar monitoring stations along the Whangaehu River.

The time (since lahar arrival) when Crater Lake water of mass M_0 has passed each location can be determined by integrating the time-variant mass flux of original Crater Lake water Q_{CLW}:

$$Q_{CLW} = F_{CLW} Q_M \,, \qquad (1)$$

where F_{CLW} is the weight percentage of original Crater Lake water in (sediment/stream water/Crater Lake water suspension) lahar dip samples and Q_M is the time-variant lahar mass flux:

$$Q_M = \rho_L Q_V \,. \qquad (2)$$

Q_V and ρ_L are time-variant lahar discharge and time-variant lahar density (taken as equal to the bulk density of dip samples), respectively. The acidic, highly mineralized and known composition of Crater Lake water immediately prior to the March 2007 lahar (Christensen et al. 2010), together with measurements of water chemistry (through Ion-chromatography and Atomic Absorption Spectroscopy; Supplementary material Table DR 1) and sediment concentration in dip samples, becomes the key for deriving time-series data of F_{CLW} as:

$$F_{CLW} = (1 - SC)\frac{C_L - C_S}{C_{CLW} - C_S} \qquad (3)$$

SC is sediment concentration in weight percent. C_L, C_S and C_{CLW} are the concentrations of chloride in dip samples, in stream water before lahar arrival and in the Crater Lake, respectively. Chloride is well suited for quantifying lahar/stream water mixing processes

because of its high solubility in neutral to acidic aqueous solutions encountered in Ruapehu lahars (e.g. Cronin et al. 1996). Synchronization is required for combining time-series data of Q_V, ρ_L and F_{CLW} to yield curves of mass fluxes for stream water, Crater Lake water and suspended sediment against time. All automatically logged data streams (seismic data, automated video and stage heights) were routinely GPS time-stamped. Manually-operated digital video footage and photographs from cameras with internal clocks were corrected to GPS time after the lahar sampling campaign. This also allowed correcting and specifying the lahar dip-sample times as the sampling procedure was captured by video and photographs. The alignment of constant-frequency time-series for Q_V and the non-constant sampling frequency time-series for ρ_L and F_{CLW} from dip-samples was achieved through cubic spline interpolation of timed ρ_L and F_{CLW} data points. Three additional time-series points were computed through cubic spline interpolation for T_A (specifiable through video and seismic data to less than 5 seconds precision), T_S (specifiable through seismic data to less than 5 seconds precision) and T_P (determined through graphical integration of Crater Lake water mass flux against time curves). These time-constraints together with maxima of Q_V and F_{CLW} in the laharic suspension allow approximating the uncertainty in the calculated values of volume of Crater Lake water in the head to be less than 2 percent.

In order to obtain E_{TOT} for each location, we compute the time-variant bulk energy flux, Q_{Etot}, as the sum of the time-variant fluxes of potential (Q_{Epot}) and kinetic energies (Q_{Epot}) through each observation point:

$$Q_{Etot} = Q_{Epot} + Q_{Ekin} = gQ_M H + \frac{1}{2} Q_M U_D^2, \qquad (4)$$

H denoting height above sea level. Data of Q_{Etot} against time t can be integrated over the time interval $[t_x, t_{x+1}]$ to yield the bulk energy of the fraction of lahar that passed the location during this time interval:

$$E_{tot}(t_X, t_{X+1}) = \int_{t_X}^{t_{X+1}} Q_{E\,tot}(t)dt\,. \qquad (5)$$

The total linear momentum P(t_x, t_{x+1}) of the fraction of lahar that passes a monitoring location between times t_x and t_{x+1} (Fig. 3C) can be computed in a similar manner by integrating curves of time-variant linear momentum flux Q_P:

$$Q_P = Q_M U_D \qquad (6)$$

and time t as:

$$P(t_X, t_{X+1}) = \int_{t_X}^{t_{X+1}} Q_P(t)dt\,. \qquad (7)$$

References cited in supplementary material:

Chow, V. T., 1959, Open channel hydraulics, McGraw-Hill, New York.

Christensen, B.W., Reyes, A.G., Young, R., Moebis, A., Sherburn, S., Cole-Baker, J., and Britten, K., 2010, Cyclic processes and factors leading to phreatic eruption events: Insights from the 25 September 2007 eruption through Ruapehu Crater Lake, New Zealand: Journal of Volcanology and Geothermal Research, v. 191, p. 15-32.

Cole, S.E., 2011, Geophysical investigation into the internal dynamics of moving lahars, Massey University (unpublished PhD Thesis), 209 pp, Massey University, New Zealand.

Cronin, S.J., Neall, V.E., Lecointre, J.A., and Palmer, A.S., 1996, Unusual "snow slurry" lahars from Ruapehu Volcano, New Zealand, September 1995: Geology, v. 24, p. 1107–1110.

Cronin, S. J., Neall, V.E., Lecointre, J.A., and Palmer, A.S., 1997, Changes in Whangaehu River lahar characteristics during the 1995 eruption sequence, Ruapehu volcano, New Zealand: Journal of Volcanology and Geothermal Research, v. 76, p. 47-61.

Dinehart, R. L., 1997, Sediment transport in the hyperconcentrated phase of the March 19, 1982, lahar, in Hydrologic consequences of hot-rock/snowpack interactions at Mount St. Helens volcano, Washington, 1982-84, edited by T. C. Pierson, pp. 37-52, United States Geological Survey.

Doyle, E.E., Cronin, S.J., and Thouret, J.C., 2011, Defining conditions for bulking and debulking in lahars: Geological Society of America Bulletin, v. 123, p. 1234-1246, DOI: 10.1130/B30227.1.

Lavigne, F., and Suwa, H., 2004, Contrasts between debris flows, hyperconcentrated flows and stream flows at a channel of Mount Semeru, East Java, Indonesia: Geomorphology, v. 61, p. 41-58.

Lube, G., Cronin, S.J., and Procter, J.N., 2009, Explaining the extreme mobility of volcanic ice-slurry flows: Geology, v. 37, p. 15-18.

Manville, V., 2001, Techniques for evaluating the size of potential dam-break floods from natural dams, Science Report, 70 pp, Institute of Geological and Nuclear Sciences, Wellington.

Pierson, T. C., and Scott, K. M., 1985, Downstream dilution of a lahar: transition from debris to hyperconcentrated streamflow: Water Resources Research, v. 21, p. 1511-1524.

Rodolfo, K. S., J. V. Umbal, R. A. Alonso, C. T. Remotigue, M. L. Paladio-Melosantos, J. H. G. Salvador, D. Evangelista, and Y. Miller, 1996, Two years of lahars on the western flank of Mount Pinatubo: Initiation, flow processes, deposits, and attendant

geomorphic and hydraulic changes, in Fire and mud: eruptions and lahars of Mount Pinatubo, Philippines, edited by C. G. Newhall and R. S. Punongbayan, pp. 989-1013, University of Washington Press, Seattle.

Scott, K. M., 1988, Origins, behavior, and sedimentology of lahars and lahar-runout flows in the Toutle-Cowlitz River system: United States Geological Survey Professional Paper, 1447-A, 1-74.